

Circuit cavity electromechanics in the strong coupling regime

J. D. Teufel*, D. Li, M. S. Allman, K. Cicak, A. J. Sirois, J. D. Whittaker, and R. W. Simmonds
National Institute of Standards and Technology, 325 Broadway, Boulder, CO 80305, USA

Demonstrating and exploiting the quantum nature of larger, more macroscopic mechanical objects would help us to directly investigate the limitations of quantum-based measurements and quantum information protocols, as well as test long standing questions about macroscopic quantum coherence [1]. The field of cavity opto- and electro-mechanics [2, 3], in which a mechanical oscillator is parametrically coupled to an electromagnetic resonance, provides a practical architecture for the manipulation [4, 5] and detection [6, 7] of motion at the quantum level. Reaching this quantum level requires strong coupling, interaction timescales between the two systems that are faster than the time it takes for energy to be dissipated [8–10]. By incorporating a free-standing, flexible aluminum membrane into a lumped-element superconducting resonant cavity, we have increased the single photon coupling strength between radio-frequency mechanical motion and resonant microwave photons by more than two orders of magnitude beyond the current state-of-the-art. A parametric drive tone at the difference frequency between the two resonant systems dramatically increases the overall coupling strength. This has allowed us to completely enter the strong coupling regime. This is evidenced by a maximum normal mode splitting of nearly six bare cavity line-widths. Spectroscopic measurements of these 'dressed states' are in excellent quantitative agreement with recent theoretical predictions [11, 12]. The basic architecture presented here provides a feasible path to ground-state cooling and subsequent coherent control and measurement of the quantum states of mechanical motion.

Despite the prevalence of mechanical oscillators in many practical technological applications, demonstrating quantum mechanical effects in these systems has proved exceedingly difficult. Originally cavity optomechanical systems [2, 3] were investigated as a way to realize or even surpass the quantum limits for displacement detection [6, 7]. More recently experimental and theoretical progress sparked renewed interest in these systems as a potentially viable medium for quantum information processing. However, in order to achieve the quantum benefits, the two disparate systems must be coupled together strongly. Strong coupling in an analogous interaction between the internal states of trapped ions and their motion led first to sideband cooling to the motional ground state [13] and subsequently to exquisite quantum control and measurement. Optomechanics strives to achieve this type of performance but with a macroscopically large mechanical oscillator whose behaviour could answer fundamental questions about the ultimate limits of quantum based measurements and the nature of reality [1]. Pioneering microwave electromechanical systems utilizing parametric transducers continue their development towards detection of gravitational waves [14, 15]. Recent progress with lithographically fabricated microwave resonators [16] has enabled sideband cooling [17–19] and near quantum limited detection [20, 21]. In addition, the incorporation of superconducting qubits [22, 23] has led to the control and measurement of a single microwave phonon [23].

One of the most difficult challenges is engineering strong parametric coupling between the photon cavity and the mechanical object whose motion we are investigating. The single photon coupling strength $g_0 = Gx_{zp}$ is the product of $G = d\omega_c/dx$, the change in the photon cavity frequency ω_c for a given displacement x , and the zero point

motion $x_{zp} = \sqrt{\hbar/2m\Omega_m}$ for a mechanical mode with angular frequency Ω_m and mass m . This suggests designing a system using a small, light mechanical object with a low resonant frequency (a soft spring constant), and whose motion drastically influences the resonant frequency of a photon cavity. Some systems have attempted to balance all three of these preferred characteristics by using silica microtoroids [24], dielectric membranes [25], or nanowires [16, 19–21]. In this work, we have incorporated a free-standing aluminum membrane into a capacitive parametric transducer to produce a coupling strength two orders of magnitude larger than obtained previously in a microwave circuit. This has allowed us to move entirely into a regime of strong coupling, opening a door that leads toward ground state cooling and subsequent quantum control and measurements with these systems.

Imagine two parallel metal plates of area A separated by a uniform vacuum gap d and electrically connected with a coiled wire (see Fig. 1a,b). These plates form a capacitance $C = A\epsilon_0/d$ that electrically resonates with the inductance L of the coil at an angular frequency $\omega_c = 1/\sqrt{LC}$. When the top plate is free to move a small distance $x \ll d$, then $G = d\omega_c/dx \approx -\omega_c/(2d)$. For a cavity with $\omega_c/2\pi = 10$ GHz and a plate separation of 50 nm, $G/2\pi \approx 100$ MHz/nm. This is to be contrasted with previous experiments that used very low-mass, high aspect ratio nano-wires [16, 18–21]. These wires only contribute a fraction η ($< 1/1000$) of the total capacitance so that $G = -\eta\omega_c/(2d)$. So while these wires have large zero-point motion, the sensitivity is limited to $G/2\pi < 100$ kHz/nm.

Our approach takes advantage of the large capacitance produced by suspending an aluminum membrane approximately 50 nm above an aluminum base electrode, as shown

in Fig. 1b. As described later, the sensitivity gained with this technique outweighs the reduced x_{zp} due to the comparatively massive membrane ($m=50$ pg) and increases the single photon coupling strength even beyond those achieved with optical Fabry-Pérot cavities [25–27], where $G \sim \omega_c/\ell$ and ℓ is the length of the optical cavity. The circuit is fabricated with wafer-scale optical lithographic techniques developed for creating low-loss vacuum-gap-based microwave components [28]. The nearly circular membrane is 100 nm thick and has a diameter of 15 μm allowing drumhead-like modes to resonate freely. The fundamental mode is $\Omega_m/2\pi = 10.69$ MHz giving a zero point motion of $x_{zp} = 4.1$ fm. The total capacitance $C \approx 38$ fF combined with a parallel inductance, $L \approx 12$ nH, provides a single-mode microwave cavity resonance [28] of $\omega_c/2\pi \approx 7.5$ GHz. The device is cooled to 40 mK, far below the superconducting transition temperature of aluminum. To measure the motion of the membrane, we apply microwave signals through heavily attenuated coaxial lines to the electromagnetically coupled superconducting cavity, as shown schematically in Fig. 1c. The transmitted signals are amplified with a cryogenic low-noise amplifier and demodulated at room temperature with either a commercial vector network analyzer (for characterizing the cavity mode) or a spectrum analyzer (for characterizing the mechanical mode).

Fig. 2a shows the magnitude of transmission, $|T|^2$, near the cavity resonance at sufficiently low microwave power that radiation pressure effects can be neglected. A Lorentzian fit yields a resonance frequency of $\omega_c/2\pi = 7.47$ GHz and a loaded intensity decay rate of $\kappa/2\pi = 170$ kHz. The depth of the dip at resonance shows that the circuit is overcoupled, so that the dominant source of damping is the intentional inductive coupling to the transmission line, $\kappa_{\text{ex}}/2\pi = 130$ kHz, which is much greater than the intrinsic decay rate, $\kappa_0/2\pi = 40$ kHz. The motion of the drumhead mode modulates the capacitance and thus the frequency of the electrical resonator, creating sidebands above and below the microwave drive frequency at $\omega_d \pm \Omega_m$. Fig. 2b shows the noise power of the upper sideband due to the thermal motion of the drum at its fundamental mode, $\Omega_m/2\pi = 10.69$ MHz. These data show that the mechanical resonance has an intrinsic damping rate of $\Gamma_m/2\pi = 30$ Hz and a high mechanical quality factor $Q_m = 360,000$, consistent with the tensile stress generated by thermal contractions upon cooling [16, 18, 20]. This system is in the resolved sideband regime, in which the mechanical resonance frequency is much larger than the cavity linewidth, $\Omega_m/\kappa = 63$. This is a prerequisite for sideband cooling to the ground state [8, 9] and for observing normal-mode splitting in the driven optomechanical system [8, 10].

The quantum-mechanical behavior of this parametrically coupled system is described by the interaction Hamiltonian: $H_I = -\hbar a^\dagger a g_0 (b^\dagger + b)$, where a^\dagger and b^\dagger are the creation operators for photons and phonons, respectively.

Because the motion of this drum strongly influences ω_c , microwave signals can be used not only to detect the motion of the oscillator but also to impart backaction forces on it. The radiation pressure force of the microwave drive photons gives rise to “optical” spring and damping effects [4, 5]. The interaction Hamiltonian can be linearized in a frame co-rotating with the drive, taking the form: $H_I = -\hbar g (a^\dagger + a)(b^\dagger + b)$, where $g = g_0 \sqrt{n_d}$ is the linearized optomechanical coupling rate [8–10], and n_d is the number of drive photons in the cavity. If the drive is detuned so that its upper mechanical sideband is near the cavity resonance, $\delta = (\omega_d + \Omega_m) - \omega_c \ll \Omega_m$ as shown in Fig 2c, the modified mechanical resonance frequency Ω'_m and damping rate Γ'_m closely follow the imaginary and real parts of the cavity response. In the resolved sideband regime these quantities are well approximated by [8, 9]:

$$\Omega'_m \approx \Omega_m + \frac{4g^2\delta}{\kappa^2 + 4\delta^2}, \quad (1)$$

$$\Gamma'_m \approx \Gamma_m + \frac{4g^2\kappa}{\kappa^2 + 4\delta^2}. \quad (2)$$

Fig. 2d shows the measured effects of this dynamical backaction on the drum as a function of δ . The incident microwave power P_{in} is held constant at 10 pW. As this power is applied very far from the cavity resonance, it results in a greatly reduced number of photons in the cavity, given by $n_d = 2P_{\text{in}}\kappa_{\text{ex}}/\hbar\omega_d(\kappa^2 + 4\Delta^2)$, where $\Delta = \omega_d - \omega_c$. Even for this moderate power microwave drive with $n_d \leq 800$, the effects on the mechanical oscillator are quite striking; the intrinsic mechanical damping is dominated by the damping from the microwave photons. Fitting these results to Eqs. 1 and 2 (shown in black) gives $G/2\pi = 56$ MHz/nm while showing overall excellent agreement with the theoretical predictions.

Just as the microwave photons strongly affect the mechanical mode, the symmetry of the parametric interaction suggests that the mechanics should influence the cavity mode. To investigate this, we apply both a microwave drive tone ω_d and a second probe tone ω_p . Here the drive tone will induce an interaction between the mechanics and the cavity, while the probe tone will monitor the response of the cavity. This technique provides a way to measure the spectroscopy of the “dressed” cavity states in the presence of the electromechanical interaction. Fig. 3a shows a series of cavity probe spectra taken with successively higher microwave power applied with $\Delta = -\Omega_m$. Once the drive power is large enough that $g \sim \sqrt{\Gamma_m\kappa}$, the mechanical sideband of the driving field appears in the cavity response function. As n_d , and hence g , increase so does the normalized probe transmission at the cavity resonance, $|T(\omega_c)|$. The width of this peak also increases and is given by the modified mechanical damping rate in Eq. 2. This electromechanical effect can be understood as the result of a radiation pressure force at the beat frequency between the drive and probe photons, which drives the motion of the

drum near its resonance frequency. The driven motion results in a mechanical sideband on the the drive field that can interfere with the probe field and hence a modified probe spectrum. This interference is the mechanical analogue of electromagnetically induced transparency [29] well known in atomic physics, and has only recently been addressed in the context of optomechanics, both theoretically [11, 12] and experimentally [12]. Applying this theory to our electrical circuit implies that the transmission spectrum is

$$T = 1 - \frac{\kappa_{\text{ex}}(1 - j\chi)}{\kappa + 2j(\omega_p - \omega_c) + 4\chi(\omega_d - \omega_c)}, \quad (3)$$

where

$$\chi = \frac{4g^2\Omega_m}{[\kappa + 2j(\omega_p - 2\omega_d + \omega_c)][\Omega_m^2 - (\omega_p - \omega_d)^2 + j(\omega_p - \omega_d)\Gamma_m]}.$$

At high enough power, Γ'_m becomes comparable to or greater than κ , at which point Eqs. 1 and 2, are no longer valid. This is precisely the point at which the driven system enters the strong coupling regime, where the coupling exceeds the intrinsic dissipation in either of the original modes ($g \geq \kappa \gg \Gamma_m$). The eigenmodes of the driven, coupled system are now hybrids of the original radio-frequency mechanical and microwave electrical resonances. The system exhibits the well-known normal-mode splitting of two strongly coupled harmonic oscillators, as was recently demonstrated in a room-temperature optomechanical system [27]. For our device, progression into the strong coupling regime is shown in Fig. 3a,b with a crossover occurring at $n_d \sim 10^5$. In this regime, the damping rate of each of the two normal modes approaches $(\kappa + \Gamma_m)/2$, and the coupling results in a splitting of $2g$. In Fig. 3c, g is extracted by fitting each spectrum at a given drive power to Eq. 3. The splitting shows the expected $\sqrt{n_d}$ dependence with a single photon coupling rate of $g_0/\pi = 460$ Hz. At the highest drive power, $n_d = 5 \times 10^6$, the splitting is $g/\pi = 1$ MHz, exceeding both κ and Γ_m .

By measuring the in-phase and quadrature components of the transmitted probe signal, we determine the real and imaginary parts of the cavity spectrum in the presence of the electromechanical interactions. We find excellent agreement between theory and experiment for both magnitude and phase over the entire range of accessible detunings and powers. Fig 4a shows the magnitude and phase of the probe transmission for three arbitrary values of δ when $g/\pi = 150$ kHz. The black lines are fits to the magnitude and argument of Eq. 3. Two-dimensional plots of $|T|$ are shown in Fig. 4 as a function of both ω_d and ω_p . At low drive amplitude (Fig. 4b), the narrow mechanical sideband appears as a sharp dip or peak in transmission whenever $\omega_p = \omega_d + \Omega'_m$. As the drive amplitude is increased (Fig. 4c), the dispersive coupling between the normal modes becomes apparent. While the mechanical sideband is narrow when it is far from resonance, as it approaches ω_c , it inherits the cavity's larger damping rate. At the largest coupling, the normal mode splitting is appreciable for a broad range of drive and probe frequencies as shown in Fig. 4d.

Assuming thermal equilibrium with the cryostat temperature of 40 mK, the thermal population of the microwave cavity n_c and the mechanical mode n_m would be 10^{-4} and 80 quanta, respectively. Although the measurements shown here do not distinguish between classical or quantum behavior, this system possesses the coupling strength and low thermal decoherence rates necessary to realize quantum entanglement between the mechanical and electromagnetic modes. With the cavity initially in its quantum-mechanical ground state, the strong coupling implies that resolved sideband cooling can be used to reduce the occupancy of the mechanical mode by a factor of $\kappa/\Gamma_m \approx 5000$ [8–10], placing both (coupled) resonators in their ground state. This is the quantum-enabled regime in which the thermal decoherence rate is $\Gamma_{\text{th}} = \bar{n}_m\Gamma_m \ll \kappa \ll \Omega_m$. Strongly coupled quantum harmonic oscillators pave the way for many future experiments, including quantum information processing and storage, and the generation of nonclassical states of both the photon and phonon fields [2, 3, 30].

This experiment demonstrates the greatly improved electromechanical coupling that is possible by engineering a microwave resonant circuit to include a micromechanical membrane. We have shown quantitative agreement with the theoretical predictions for dynamical backaction. The parametric interaction allows for strong coupling between two harmonic modes, at ~ 11 MHz and ~ 7.5 GHz, far off resonance with each other, with an energy transfer rate much faster than the energies decays from either system. Just as electromagnetically induced transparency enabled such innovations as slow light and photon storage, the analogous electromechanical effects demonstrated here should already give rise to group delay in microwave signals of $\Gamma_m^{-1} \approx 5$ ms and storage of microwave quantum states on the timescale of $\Gamma_{\text{th}}^{-1} \approx 70 \mu\text{s}$ [12]. Future experiments, incorporating an even lower noise microwave amplifier [20, 31] into the measurement, will facilitate measurements of the thermal population at the single-phonon and single-photon level, and could allow Heisenberg-limited detection of displacement or force with sensitivities at the attometer and attonewton level. Lastly, straightforward integration of this electromechanical circuit with superconducting qubits [28] will lead to generation and manipulation of motional quantum states [23].

ACKNOWLEDGEMENTS

We thank A. W. Sanders for taking the micrograph in Fig. 1b, and gratefully acknowledge discussions with T. Donner, J. H. Harlow and K. W. Lehnert. This work was financially supported by NIST and DTO. Contribution of the U.S. government, not subject to copyright. Correspondence should be addressed to J.D.T (john.teufel@nist.gov).

-
- [1] W. Marshall, C. Simon, R. Penrose, and D. Bouwmeester, *Phys. Rev. Lett.*, **91**, 130401 (2003).
- [2] T. J. Kippenberg and K. J. Vahala, *Science*, **321**, 1172 (2008).
- [3] F. Marquardt and S. M. Girvin, *Physics*, **2**, 40 (2009).
- [4] V. B. Braginsky and A. B. Manukin, *Sov. Phys. JETP*, **25**, 653 (1967).
- [5] M. I. Dykman, *Sov. Phys. Solid State*, **20**, 1306 (1978).
- [6] V. B. Braginsky and Y. I. Vorontsov, *Soviet Physics Uspekhi*, **17**, 644 (1975).
- [7] C. M. Caves, *Phys. Rev. D*, **23**, 1693 (1981).
- [8] F. Marquardt, J. P. Chen, A. A. Clerk, and S. M. Girvin, *Phys. Rev. Lett.*, **99**, 093902 (2007).
- [9] I. Wilson-Rae, N. Nooshi, W. Zwerger, and T. J. Kippenberg, *Phys. Rev. Lett.*, **99**, 093901 (2007).
- [10] J. M. Dobrindt, I. Wilson-Rae, and T. J. Kippenberg, *Phys. Rev. Lett.*, **101**, 263602 (2008).
- [11] G. S. Agarwal and S. Huang, *Phys. Rev. A*, **81**, 041803 (2010).
- [12] R. Weis, R. Riviere, D. Deleglise, E. Gavartin, O. Arcizet, A. Schliesser, and T. J. Kippenberg, arXiv:1007.0565 (2010).
- [13] F. Diedrich, J. C. Bergquist, W. M. Itano, and D. J. Wineland, *Phys. Rev. Lett.*, **62**, 403 (1989).
- [14] V. B. Braginsky, A. B. Manukin, and M. Y. Tikhonov, *Sov. Phys. JETP*, **31**, 829 (1970).
- [15] N. P. Linthorne, P. J. Veitch, and D. G. Blair, *Journal of Physics D: Applied Physics*, **23**, 1 (1990).
- [16] C. A. Regal, J. D. Teufel, and K. W. Lehnert, *Nat Phys*, **4**, 555 (2008).
- [17] K. R. Brown, J. Britton, R. J. Epstein, J. Chiaverini, D. Leibfried, and D. J. Wineland, *Phys. Rev. Lett.*, **99**, 137205 (2007).
- [18] J. D. Teufel, J. W. Harlow, C. A. Regal, and K. W. Lehnert, *Phys. Rev. Lett.*, **101**, 197203 (2008).
- [19] T. Rocheleau, T. Ndukum, C. Macklin, J. B. Hertzberg, A. A. Clerk, and K. C. Schwab, *Nature*, **463**, 72 (2010).
- [20] J. D. Teufel, T. Donner, M. A. Castellanos-Beltran, J. W. Harlow, and K. W. Lehnert, *Nat Nano*, **4**, 820 (2009).
- [21] J. B. Hertzberg, T. Rocheleau, T. Ndukum, M. Savva, A. A. Clerk, and K. C. Schwab, *Nat Phys*, **6**, 213 (2010).
- [22] M. D. LaHaye, J. Suh, P. M. Echternach, K. C. Schwab, and M. L. Roukes, *Nature*, **459**, 960 (2009).
- [23] A. D. O'Connell, M. Hofheinz, M. Ansmann, R. C. Bialczak, M. Lenander, E. Lucero, M. Neeley, D. Sank, H. Wang, M. Weides, J. Wenner, J. M. Martinis, and A. N. Cleland, *Nature*, **464**, 697 (2010).
- [24] A. Schliesser, O. Arcizet, R. Riviere, G. Anetsberger, and T. J. Kippenberg, *Nat Phys*, **5**, 509 (2009).
- [25] J. D. Thompson, B. M. Zwickl, A. M. Jayich, F. Marquardt, S. M. Girvin, and J. G. E. Harris, *Nature*, **452**, 72 (2008).
- [26] O. Arcizet, P.-F. Cohadon, T. Briant, M. Pinard, and A. Heidmann, *Nature*, **444**, 71 (2006).
- [27] S. Groblacher, K. Hammerer, M. R. Vanner, and M. Aspelmeyer, *Nature*, **460**, 724 (2009).
- [28] K. Cicak, D. Li, J. A. Strong, M. S. Allman, F. Altomare, A. J. Sirois, J. D. Whittaker, J. D. Teufel, and R. W. Simmonds, *Appl. Phys. Lett.*, **96**, 093502 (2010).
- [29] K.-J. Boller, A. Imamolu, and S. E. Harris, *Phys. Rev. Lett.*, **66**, 2593 (1991).
- [30] U. Akram, N. Kiesel, M. Aspelmeyer, and G. J. Milburn, *New Journal of Physics*, **12**, 083030 (2010).
- [31] M. A. Castellanos-Beltran, K. D. Irwin, G. C. Hilton, L. R. Vale, and K. W. Lehnert, *Nat Phys*, **4**, 929 (2008).

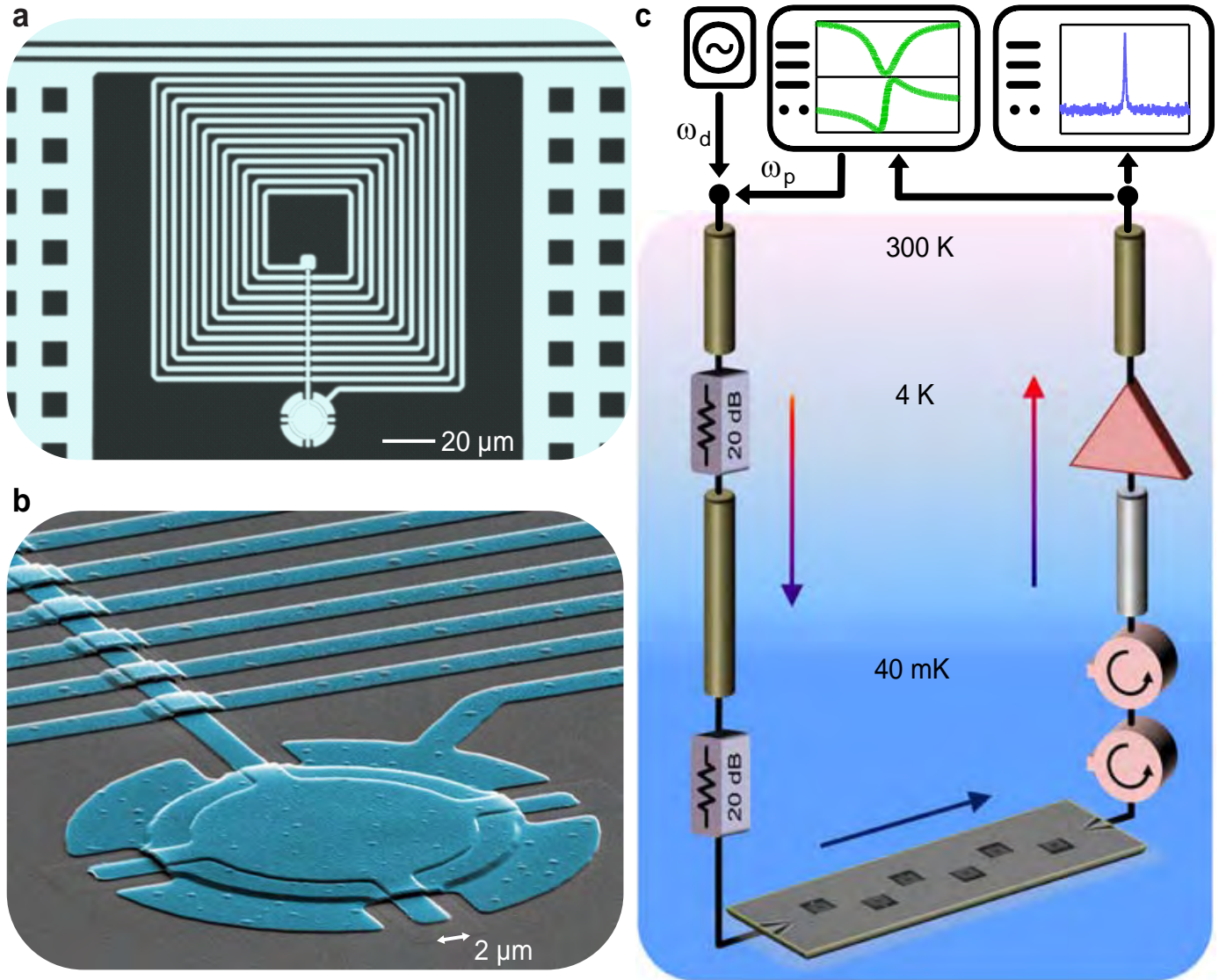


FIG. 1. **Schematic description of the experiment.** **a**, Colorized optical micrograph of the microwave resonator formed by a spiral inductor shunted by a parallel-plate capacitor. **b**, Colorized scanning electron micrograph shows the upper plate of the capacitor is suspended ~ 50 nm above the lower plate and is free to vibrate like a taut, circular drum. The metallization is sputtered aluminum (blue) patterned on a sapphire substrate (black). **c**, This circuit is measured by applying microwave signals near the electrical resonance frequency through resistive coaxial lines. The outgoing signals, in which the mechanical motion is encoded as modulation sidebands of the applied microwave tone, is coupled to a low noise, cryogenic amplifier via a superconducting coaxial cable. Cryogenic attenuators on the input line and isolators on the output line ensure that thermal noise is reduced below the vacuum noise at microwave frequencies.

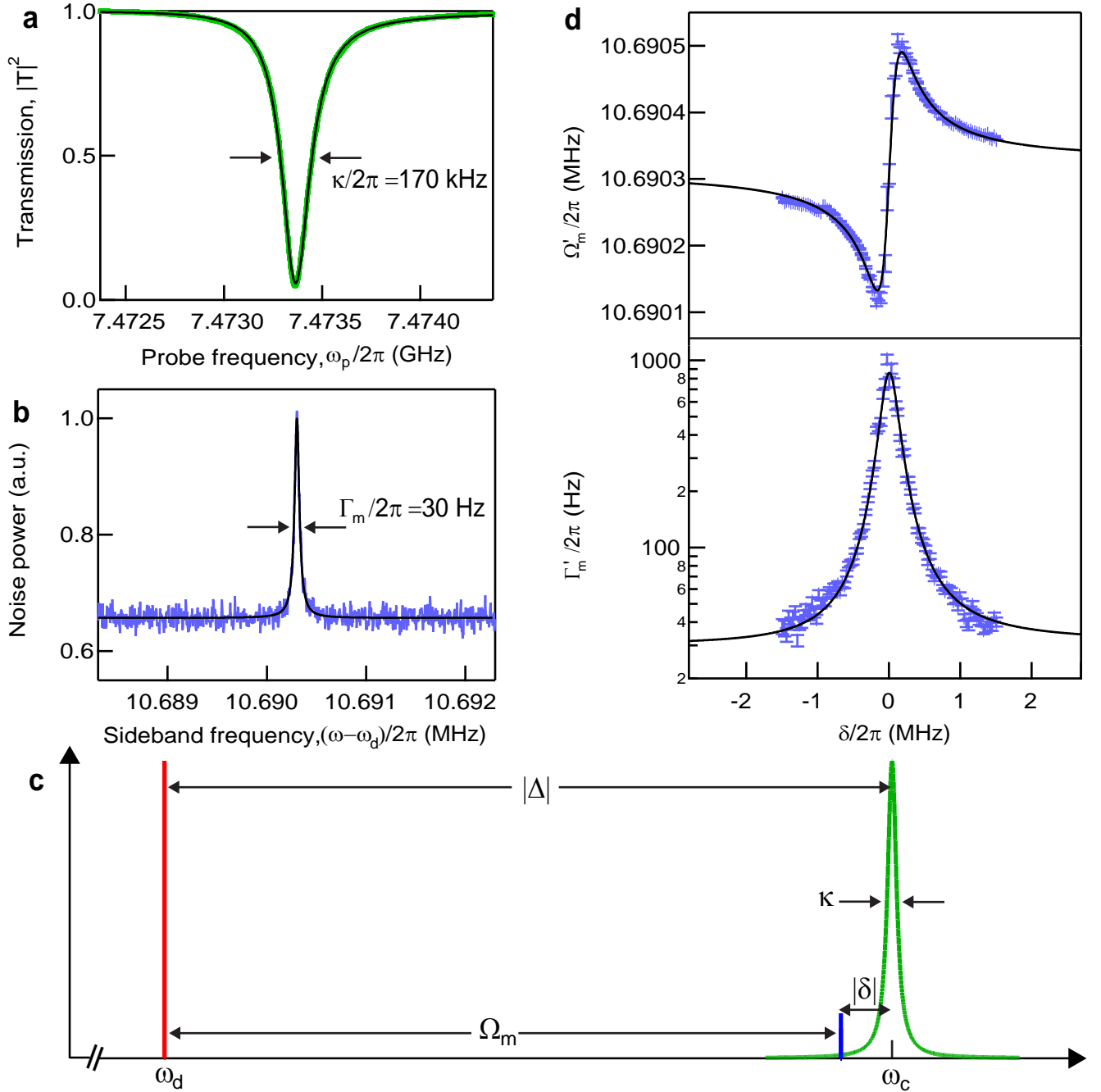


FIG. 2. **Characterization of mechanical and microwave resonances.** **a**, Measured probe transmission spectrum (green) and Lorentzian fit (black) of the microwave circuit at low power, where optomechanical effects are negligible. The width of the resonance yields the overcoupled, intensity decay rate $\kappa/2\pi=170$ kHz. **b**, The mechanical resonance manifests itself as a peak in the noise spectrum (blue), which appears Ω_m above and below the microwave drive frequency, due to the thermal motion of the drum up- or down-converting microwave photons. At low microwave power, where backaction effects are negligible, the Lorentzian fit (black) yields an intrinsic mechanical dissipation rate $\Gamma_m/2\pi=30$ Hz ($Q_m=360,000$). **c**, Schematic diagram for the relative frequencies of the microwave drive (red) and the upper mechanical sideband (blue) with respect to the narrow cavity resonance (green). **d**, The modified mechanical resonance frequency Ω'_m and damping rate Γ'_m as a function of the relative detuning δ fit well to the theory of dynamical backaction (black), yielding $G/2\pi=56$ MHz/nm.

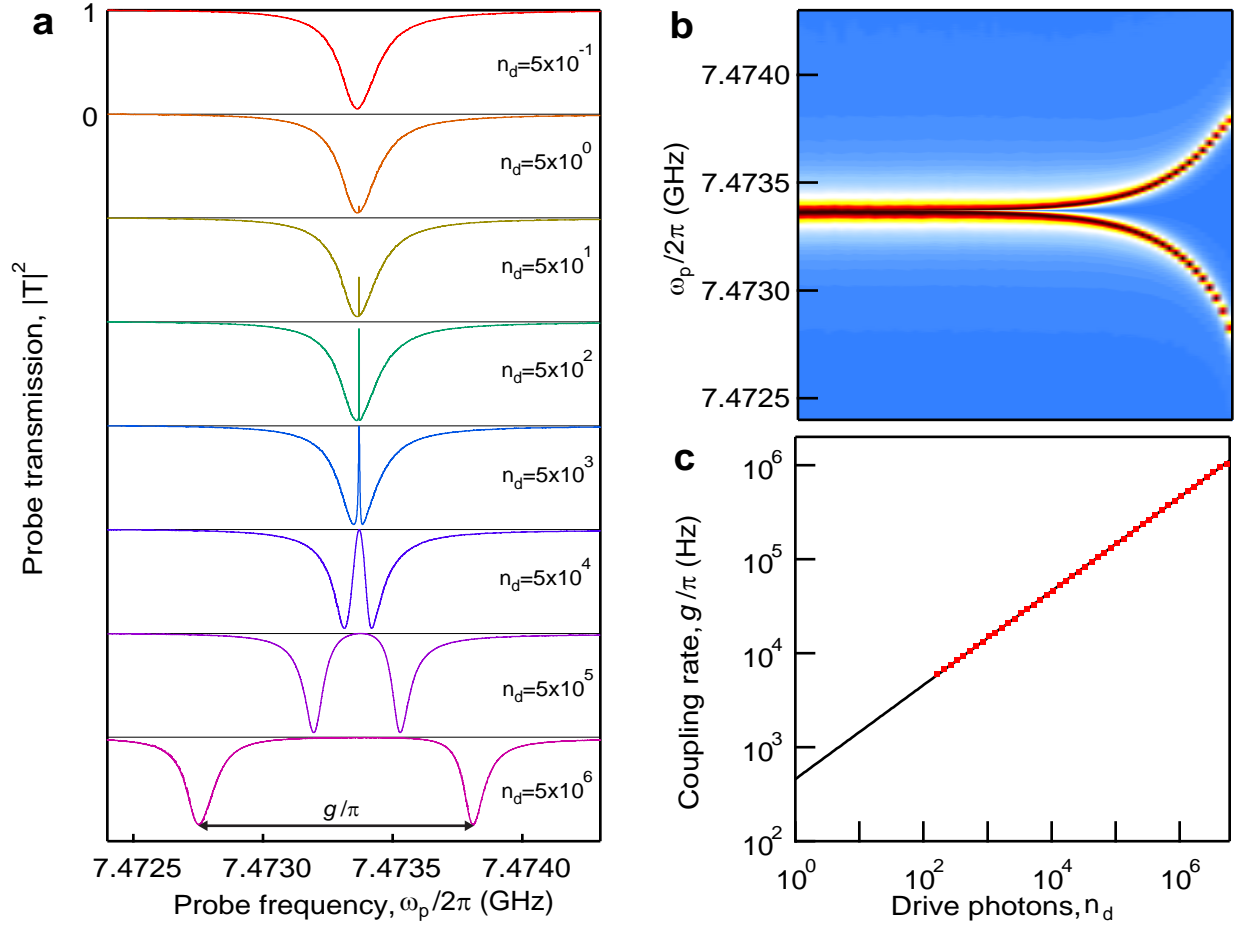


FIG. 3. **Demonstration of the strong-coupling regime.** **a**, Normalized microwave cavity transmission in the presence of a microwave drive applied with $\Delta = -\Omega_m$, with successive plots for increasing drive amplitude n_d . At moderate drive amplitude ($n_d \approx 10$), the interference between the drive and probe photons results in a narrow peak in the cavity spectrum, whose width is given by the mechanical linewidth Γ'_m . When Γ'_m becomes comparable to κ , the cavity resonance splits into normal modes. The eigenmodes of the system are no longer purely electrical or mechanical, but are a pair of hybrid electromechanical resonances. **b**, The transmission as a function of probe frequency and number of drive photons shows that the driven system enters the strong coupling regime ($g \geq \kappa, \Gamma_m$). Here, the logarithmic color scale shows the transmission as it varies from -13 dB (dark red) to 0 dB (blue). **c**, The measured coupling rate g (red) follows the expected dependence on the number of drive photons, with a fit to $\sqrt{n_d}$ shown in black.

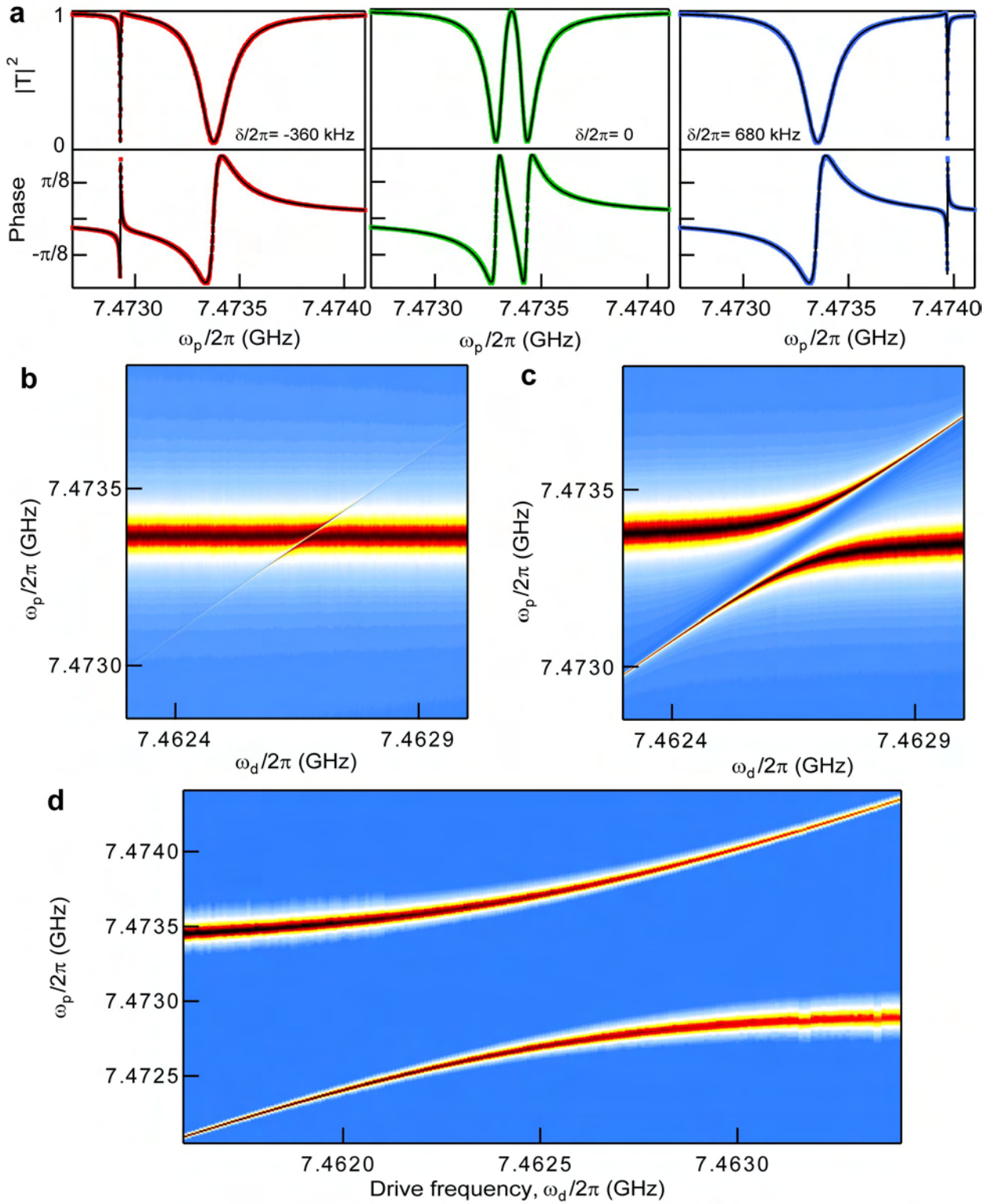


FIG. 4. **Spectroscopy in the strong-coupled regime.** **a**, The normalized magnitude and phase of the cavity transmission in the presence of a strong microwave drive. The data shown in red, green and blue are for three different detunings δ with fits to Eq. 3 (black). **b**, For relatively low drive power ($n_d \approx 10$), the mechanical sideband appears as a sharp dip in the transmission at a frequency $\omega_d + \Omega'_m$. **c**, When the drive amplitude is increased ($n_d \approx 10^4$), the two resonances show an avoided crossing between the eigenmodes of the coupled system. **d**, For the largest amplitude drive ($n_d \approx 5 \times 10^6$), the driven transmission spectra are split by much more than κ or Γ_m for a broad range of detunings.